Research Article J. Electrochem. Sci. Technol., **2023**, *14(1), 21-30*

The Ways for Bi on Pt to Enhance Formic Acid Oxidation

Hyein Lee, Young Jun Kim, Youngku Sohn, and Choong Kyun Rhee*
Department of Chemistry, Chungnam National University, Daejeon, 34134, Republic of Korea

ABSTRACT

This work presents a correlation between the behavior of formic acid oxidation (FAO) on various Bi-modified Pt(poly) disk electrodes and their morphologies observed on Bi-modified Pt(111) disk electrodes using electrochemical scanning tunneling microscopy (EC-STM) to understand the effects of Bi on Pt. To distinguish the FAO activities of Bi on Pt and plain Pt around Bi, additional Pt was intentionally deposited using two different routes: direct route and iodine route. In direct route, Pt was directly deposited on Bi islands and plain Pt sites around Bi islands, while in iodine route, Pt was exclusively deposited on Bi islands by protecting plain Pt sites with adsorbed iodine. Thus, a comparison of FAO performances on the two Bi-modified Pt electrodes with additional Pt (deposited in the different ways) disclosed a difference in FAO performances on plain Pt sites and Bi islands. When Bi coverage was ~0.04, the Bi deposits were scattered Bi islands enhancing FAO on Pt(poly). The additional Pt deposits using direct route increased FAO efficiency, while the ones using iodine route slightly decreased FAO current. The EC-STM observations indicated that Pt deposits around Bi islands, not on Bi islands, were responsible for the FAO current increase on Bi-modified Pt(poly). The FAO efficiency on Bi-modified Pt(poly) with a Bi coverage of ~0.25 increased by a factor of 2. However, the additional Pt deposits using the two Pt deposition routes notably decreased the FAO current. The dependency of FAO on Bi coverage was discussed in terms of electronic effect and ensemble effect.

Keywords : Platinum, Bismuth, Formic acid, Scanning Tunnelling Microscopy

Received : 30 June 2022, Accepted : 13 August 2022

1. Introduction

Electrochemical oxidation of formic acid has drawn an attention in fundamental science and fuel cell technology. In a scientific point of view, formic acid oxidation (FAO) on Pt-based electrochemical catalyst, a model reaction of small organic molecules, has been known to take place via dual path mechanism [1-6]: dehydrogenation ($HCOOH \rightarrow CO_2 + 2H^+ + 2e$), and dehydration ($HCOOH \rightarrow H_2O$ + poisonous CO; poisonous $CO + H_2O \rightarrow CO_2 + 2H^+ + 2e$ at a high potential). In a technical point of view, on the other hand, formic acid is one of potential fuels for portable devices and power sources at off-grid locations along with the technical advances in converting CO_2 to formic acid [7-11].

*E-mail address: ckrhee@cnu.ac.kr

DOI: https://doi.org/10.33961/jecst.2022.00514

This is an open-access article distributed under the terms of the Creative Commons Attribution Non-Commercial License (http://creativecommons.org/licenses/by-nc/4.0) which permits unrestricted non-commercial use, distribution, and reproduction in any medium, provided the original work is properly cited.

Pt-based electrochemical catalysts have been intensively investigated toward enhancement of FAO [12-17]. The main strategy was to suppress the dehydration path (forming catalytic poisons) and simultaneously to enhance the dehydrogenation path by modifying the physicochemical properties of Pt by alloying with other secondary metals like Au, Bi and Pb or by attaching the secondary metals on Pt surfaces [18-29].

Modification of Pt surfaces with Bi is one of the intensively studied examples toward FAO enhancement. For instance, irreversibly adsorbed Bi on Pt nanoparticles and Pt deposits on Au nanoparticles increased FAO performance by factor of 5 [30]. Furthermore, additional deposition of Pt on such Bi-modified Pt nanoparticles increased the catalytic efficiency by factor of 3 as well as catalytic durability in comparison to simple Bi-modified Pt nanoparticles [31]. On the other hand, a direct formic acid fuel cell stack of 35 membrane electrode assemblies using Bi-modified Pt nanoparticles was reported to generate a power of 300 W [32]. Certainly, Bi on Pt promotes

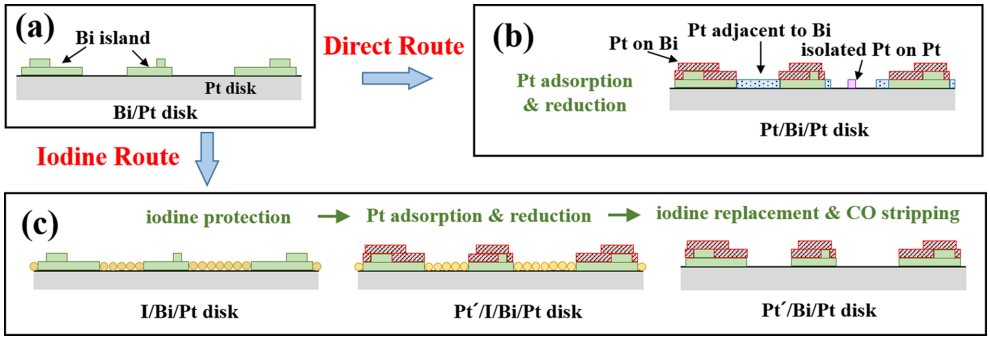

Fig. 1. Schematic illustrations of direct route and iodine route. (a) A starting surface of Bi/Pt disk, (b) Pt/Bi/Pt disk via direct route, and (c) Pt′/Bi/Pt disk via iodine route.

FAO by enhancing dehydrogenation path and simultaneously prohibiting dehydration path.

The role of Bi on Pt in FAO enhancement has been suggested in three different aspects. The first one is that Bi adatoms of a partial positive charge on Pt decrease the activation energy of dehydrogenation path by promoting the C-H bond cleavage to formate [25,26]. The second one is that adsorbed Bi aggregates divide a wide Pt surface to small domains exclusively permitting dehydrogenation (ensemble effect) [21,33]. This particular effect has been suggested to be consistent with FAO enhancement on Pt islands in a nanometer scale on inert Au surfaces [30,34,35]. The last one is electronic effect for Bi adatoms to modify the electronic properties of Pt to increase the scission of HOOC-H bond rather than that of HO-OCH bond [21]. Although the three suggestions are highly likely, no direct experimental evidence is available yet.

The aim of this work is to provide experimental evidences regarding the role of Bi on Pt in FAO enhancement. The employed strategy is to prepare various Bi-modified Pt surfaces in a controlled manner and to correlate their FAO performances to the morphologies observed using electrochemical scanning tunnelling microscopy (EC-STM).

The various Bi-modified Pt electrodes studied in this work are illustrated schematically in Fig. 1. The starting surface is a Pt disk partially covered with Bi islands, prepared by the irreversible adsorption of Bi (Bi/Pt(disk), Fig. 1(a)). Additional Pt is to deposit on Bi/Pt(disk) to understand FAO on Pt directly contacting with Bi islands. To achieve the specific purpose, two routes additionally depositing Pt on Bi/Pt(disk) are designed as illustrated in Fig. 1(b) and (c), respectively. In direct route (Fig. 1(b)), additional Pt would deposit on two different places: Bi islands and plain Pt sites around Bi islands [31,36]. The FAO behavior on this particular Pt-modified Bi/Pt disk (designated Pt/Bi/Pt disk) is anticipated to simultaneously come from the Pt deposits on Bi islands and the Pt deposits on plain Pt sites. In iodine route suggested in this work (Fig. 1(c)), meanwhile, an iodine adsorption step precedes additional Pt deposition to protect the plain Pt sites from solution exposure; consequently, only the Bi islands are subject to Pt deposition. Specifically, iodine adsorbs on plain Pt sites during a contact of Bi/Pt disk with an iodide solution, and a subsequent immersion of the iodine-protected Bi/Pt(disk) (I/Bi/Pt(disk)) into a Pt precursor solution allows the irreversible adsorption of Pt ions only on Bi islands. An electrochemical reduction following a brief rinsing turns the adsorbed Pt ionic layers to metallic layers (Pt′/I/Bi/Pt(disk)). Here, it should be noted that the adsorbed iodine on I/Bi/Pt(disk) and Pt′/I/Bi/Pt(disk) provides another dimension in understanding FAO. In the presence of adsorbed iodine, specifically, the Bi islands of Bi/Pt(disk) and the Pt deposits on Bi islands of Pt′/I/Bi/Pt(disk) (Fig. 1(c)) would be the sites available to FAO. The adsorbed iodine on Pt′/I/Bi/Pt(disk) can be removed by replacing with CO, which is sequentially stripped off. Because CO is oxidized at a lower potential than adsorbed iodine, such a CO replacement procedure [37,38] is not to strip Bi deposits as demonstrated in Fig. S1 and S2, Supporting Information. On the final Pt-covered Bi/Pt(disk) of iodine route (Fig. 1(c)), Pt′/Bi/Pt(disk), FAO will take place on two different Pt sites again: the Pt deposits on Bi islands and the plain Pt sites of the Pt disk substrate. Therefore, the several

Bi-modified Pt disk electrodes as illustrated in Fig. 1 may distinguish possible FAO sites to elucidate the role of Bi.

2. Experimental

Two different Pt disk electrodes were used in this work. One was a Pt single crystal bead of ~2 mm in diameter, obtained by melting a Pt wire (0.5 mm diameter, 99.99%, Aldrich) in a hydrogen and oxygen flame. One of the (111) facets (Pt(111)), confirmed with the reflection patterns of a He-Ne laser, was employed for EC-STM measurements. The other was a polycrystalline Pt disk (Pt(poly)), acquired by cutting a bead crystal in a random direction to a hemisphere and polishing with a 0.25 μm diamond paste. Pt(poly) was used for electrochemical and XPS measurements. Both Pt disk electrodes were annealed in a hydrogen flame to obtain clean surfaces before being modified.

For the irreversible adsorption of Bi or Pt, the Pt disk electrodes were immersed into a precursor solution for 10 min without potential control. The precursor solutions of Bi and Pt were 0.10 M H_2SO_4 (Suprapur, Merck) solutions of 0.13 mM Bi^{3+} and 0.10 mM of Pt^{2+} obtained by dissolving Bi_2O_3 (99.999%, Aldrich) and K_2PtCl_4 (98%, Aldrich), respectively. After the irreversible adsorption step followed by a brief rinse with water, the adsorbed ionic layers were electrochemically reduced at 0.1 V in 0.10 M H_2SO_4 solution for 10 min. On the other hand, iodine adsorption was performed by immersing a Bi-modified Pt electrode into a solution of 0.10 M KI (> 99.0%, Aldrich) for 20 min without potential control. Removal of adsorbed iodine was carried out by replacing adsorbed iodine with CO and subsequently stripping the adsorbed CO. Specifically, the adsorbed iodine was replaced with CO during a contact of an iodine-covered Pt surface with CO-saturated 0.10 M H_2SO_4 solution at 0.1 V for 15 min, and the adsorbed CO was sequentially stripped off by holding at 0.4 V in a CO-free 0.10 M H_2SO_4 solution for 20 min. The detailed voltammograms concerning iodine removal with CO are presented in Fig. S1 and S2, Supporting Information.

EC-STM measurements were performed using an STM instrument (Nanoscope V, Veeco Inc.) operated at the condition of 0.1 V sample potential, 0.01 V tip potential and 0.8 nA tunneling current in 0.10 M H_2SO_4 solution with a polyethylene-coated tungsten tip.

In electrochemical and EC-STM experiments, the potential was controlled using a three-electrode system. The reference and counter electrodes were a home-made Ag/AgCl electrode in 1.0 M NaCl solution and a Pt counter wire, respectively. All potentials reported in this work are the values measured against the reference electrode. The scan rate for voltammetry was 50 $mV \cdot s^{-1}$.

The surface area of a Pt(poly) electrode was calculated using the measured charges of hydrogen adsorption (Q_H/210 $\mu C \cdot cm^{-2}$) and CO stripping (Q_{CO}/420 $\mu C \cdot cm^{-2}$) in 0.10 M H_2SO_4 solution. In FAO measurements, only the polished surface of Pt(poly) disk was exposed to a mixed solution of 1.0 M formic acid (98%, Wako) and 0.10 M H_2SO_4 by maintaining a meniscus position.

The Bi coverages (*i.e.*, the mole ratios of adsorbed Bi atoms to surface Pt atoms) were estimated using two different methods. One was to measure the hydrogen charge (Q_H) of a Bi-modified Pt(poly) and to convert to a Bi coverage using the following equation: Bi coverage = $(Q_{H,\ plain\ Pt(poly)} - Q_{H,\ Bi/Pt(poly)})/(3Q_{H,\ plain\ Pt(poly)})$, assuming that a Bi atom prohibits three Pt atoms from hydrogen adsorption [39,40]. The other was to measure the area fraction covered by Bi in an STM image using a bearing function provided by the manufacturer of the employed STM instrument. The area fraction of Bi on a Bi-modified Pt(111) was converted to Bi coverage using a conversion factor of 1/4, because of the $(\sqrt{2} \times 2\sqrt{2})$ unit cell of Bi on Pt(111) [21,33]. It should be noted here that the bearing function was also utilized to estimate the area fractions of the deposits on Pt(111) as a function of stacking height in the unit of atomic-layer.

An X-ray photoelectron spectrometer (XPS, K-Alpha+ XPS spectrometer, Thermo Scientific Co.) was employed to determine the atomic ratio of Bi and Pt. Photoelectrons were generated using an Al K_α X-ray beam (1486.7 eV), and the photoelectron energies were measured using a multichannel hemispherical electron energy analyzer operated at a constant pass energy of 50 eV.

3. Results and Discussion

3.1 STM images of Pt/Bi/Pt(111) and Pt′/Bi/Pt(111)

Fig. 2 presents typical STM images of various Pt(111) surfaces modified with Bi and Pt. Fig. 2(a) is

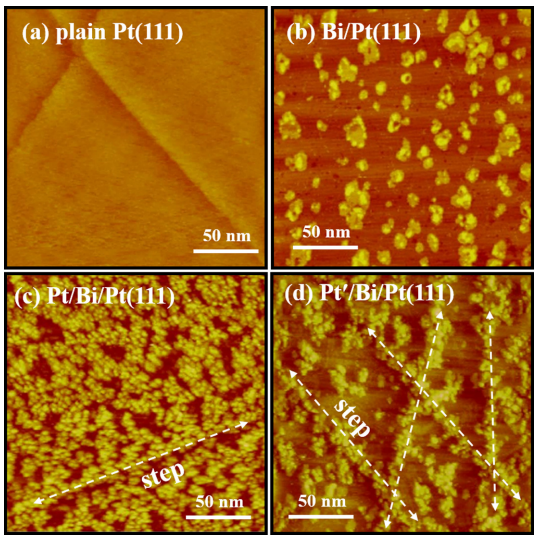

Fig. 2. EC-STM images of (a) plain Pt(111), (b) Bi/Pt(111), (c) Pt/Bi/Pt(111), and (d) Pt′/Bi/Pt(111).

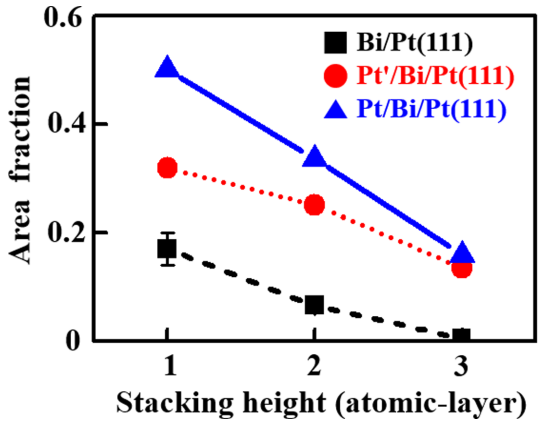

Fig. 3. The area fractions of various deposits on Pt(111) as a function of stacking height in the unit of atomic-layer. The area fraction is defined as a ratio of the area occupied by a layer of a certain stacking height to the whole area in an STM image.

an image of plain Pt(111). Application of direct route on a Pt(111) disk did not induce any change in STM image, indicating no adsorption of Pt ions on plain Pt(111). After deposition of Bi on Pt(111) disk, scattered Bi islands are clearly visible on the terrace of Pt(111) in Fig. 2(b) (as well as on the steps although not shown here). The fraction of the area occupied by Bi islands is ~0.17, and the sizes of the Bi islands range from 2.0 nm to 18 nm. In addition, the brighter protrusions, mostly on the edges of large Bi islands, imply that the Bi islands are double-layered as depicted in Fig. 1(a). An STM image of Pt/Bi/Pt(111) surface after application of direct route (Fig. 2(c)) clearly demonstrates that small Pt deposits (~5 nm in diameter), distinguishing from Bi islands, are notable for the area fraction to increase to ~0.5. A comparison of the images of Bi/Pt(111) and Pt/Bi/Pt(111) clearly suggests that Pt deposits are not only on Bi islands but also around Bi islands; consequently, Pt deposits bridge Bi islands as illustrated in Fig. 1(b). More specifically, the Bi islands on the step (double headed arrow) are severely connected, while those on the terrace are randomly linked. On the other hand, the topography of Pt′/Bi/Pt(111) after application of iodine route (Fig. 2(d)) differs from that of Pt/Bi/Pt(111). Even though small Pt deposits are obviously discernable on Pt′/Bi/Pt(111), the area faction (~0.3) is much lower than that on Pt/Bi/Pt(111). In particular, the Bi islands on the terraces are covered but not seriously bridged by Pt deposits, while those on the steps are merged. These observations demonstrate that iodine protection is more effective on terrace.

Fig. 3 shows the area fractions occupied by various deposits on Pt(111) in STM images as a function of stacking height expressed in the unit of atomic-layer. The dashed line in Fig. 3 reveals that most of the Bi islands on Bi/Pt(111) are monatomic layers with a slight amount of second layers. On Pt/Bi/Pt(111), the area fractions (the solid line) increase significantly regardless of stacking height. The area fraction (~0.2) of the three atomic-layers high layers on Pt/Bi/Pt(111) is similar to that of the monatomic layers on Bi/Pt(111), implying that two atomic-layers high Pt deposits are on Bi islands. In addition, the increment of ~0.3 in the area fraction of the monatomic layers is due to Pt deposits around Bi deposits. On the other hand, the area fractions of Pt′/Bi/Pt(111) (the dotted line) differ from those of Bi/Pt(111) and Pt/Bi/Pt(111). The lower area fractions of the one and two atomic-layers high layers on Pt′/Bi/Pt(111) support that the number of Pt deposits on plain Pt sites is much less in iodine route than that in direct route. Indeed, the area fraction of the third atomic layer is similar to that of Pt/Bi/Pt(111), revealing that Pt deposits are on Bi islands,

3.2 XPS spectra of Pt/Bi/Pt(111) and Pt′/Bi/Pt(111)

Fig. 4 shows a typical XPS 4f spectra of Bi and Pt

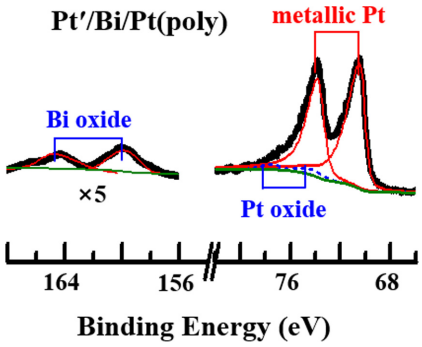

Fig. 4. Typical XPS 4f spectra of Bi and Pt on Pt′/Bi/Pt(poly).

on Pt′/Bi/Pt(poly). The chemical state of Bi is oxide, while that of Pt is almost metallic, implying that during a transfer to the XPS instrument through air, Bi is easier to be oxidized. The atomic ratio of Bi to Pt on Bi/Pt(poly) is 0.04 ± 0.01; meanwhile those on Pt′/Bi/Pt(poly) and Pt/Bi/Pt(poly) are 0.03 ± 0.01. The slight decreases in the atomic ratio, although not solid, may reflect insignificant increases in the amount of surface Pt within the sampling depth of XPS, although the Pt deposits are clearly distinguishable in Fig. 2.

3.3 Electrochemical behavior of Pt/Bi/Pt(poly) and Pt′/Bi/Pt(poly) in H_2SO_4 solution

Fig. 5 compares the cyclic voltammograms of Bi/Pt(poly), Pt/Bi/Pt(poly) and Pt′/Bi/Pt(poly) in 0.10 M H_2SO_4 solution. The dotted line cyclic voltammogram of plain Pt(poly) is presented as a reference. After application of direct route to plain Pt(poly), no change in voltammogram should be noted again. The cyclic voltammogram of Bi/Pt(poly) (Fig. 5(a)) differs from that of plain Pt(poly) in three aspects. The first one is that the hydrogen coverage (a mole ratio of adsorbed hydrogen atoms to surface Pt atoms) decreases from 1.00 ± 0.02 to 0.87 ± 0.04. The particular decrement in hydrogen coverage is equivalent to a Bi coverage of 0.04 ± 0.01. The area fraction of Bi islands on Pt(111) in Fig. 2(b) corresponds to a Bi overage of ~0.04 (~0.17/4 as explained in Experimental), close enough to the electrochemically determined Bi coverage on Pt(poly), indicating that Pt(111) and Pt(poly) are similar to each other at least regarding Bi coverage. The second one is the oxidation peak of Bi at 0.6 V, overlapping with the surface oxidation charge of Pt. The last is the appearance of Bi oxide reduction peak (indicated with an arrow) around 0.3 V at the foot of Pt oxide reduction peak (~0.4 V). Deposition of Pt on Bi/Pt(poly) using direct and iodine routes (Fig. 5(b) and (c)) slightly increases hydrogen coverage to 0.91 ± 0.05 and 0.88 ± 0.03, respectively. Although additional Pt deposits are clear in Fig. 2, the insignificant increments in hydrogen charge may be due to that hydrogen adsorption to the additionally deposited Pt is hampered by Bi. However, the additional charges of surface oxidation above 0.8 V (the shaded areas in Fig. 5(b) and (c)) are the features clearly distinguishing Pt/Bi/Pt(poly) and Pt′/Bi/Pt(poly) from Bi/Pt(poly), indicating that the oxidative behavior of Pt deposits on and around Bi islands may differ from that of plain Pt.

3.4 FAO behavior of Pt/Bi/Pt(111) and Pt′/Bi/Pt(111)

Fig. 6 compares the FAO behaviors of various Pt(poly) electrodes covered with Bi, Pt and iodine. On plain Pt(poly), the low current below 0.4 V and the small oxidation peak at ~0.6 V in the positive-

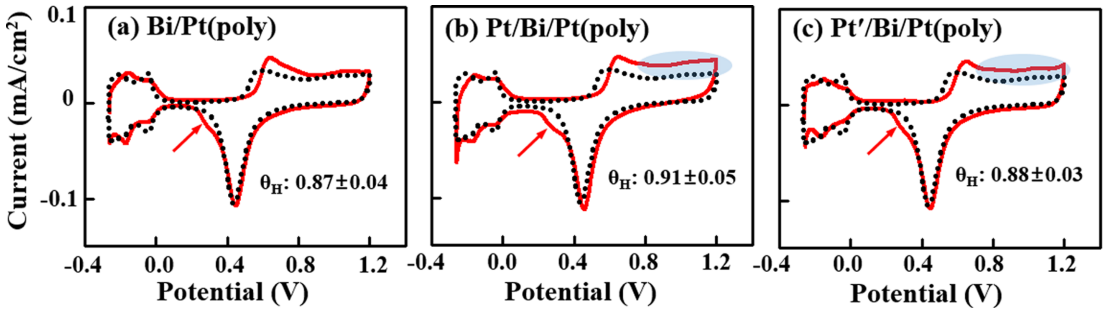

Fig. 5. Cyclic voltammograms of (a) Bi/Pt(poly), (b) Pt/Bi/Pt(poly), and (c) Pt′/Bi/Pt(poly) in 0.10 M H_2SO_4 solution. The dotted line cyclic voltammogram of plain Pt(poly) is presented as a reference. Scan rate: 50 $mV \cdot s^{-1}$.

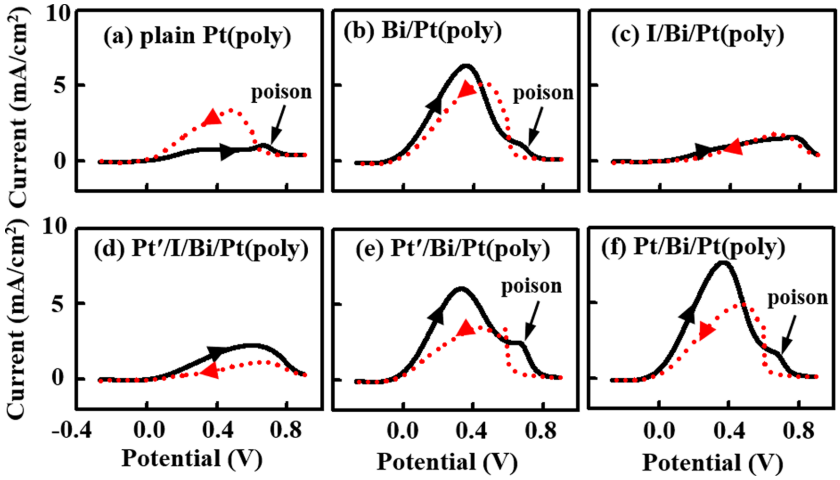

Fig. 6. FAO behaviors of various Bi-modified Pt(poly) electrodes with a Bi coverage of ~0.04 in a solution of 1.0 M formic acid and 0.10 M H_2SO_4: (a) plain Pt(poly), (b) Bi/Pt(poly), (c) I/Bi/Pt(poly), (d) Pt/I/Bi/Pt(poly), (e) Pt′/Bi/Pt(poly), and (f) Pt/Bi/Pt(poly). Scan rate: 50 $mV \cdot s^{-1}$.

going scan (Fig. 6(a)) indicate that catalytic poisons via dehydration path seriously suppress dehydrogenation path. Bi/Pt(poly) shifts the FAO onset potential to -0.15 V and increases the FAO current with a noticeable poison oxidation peak as shown in Fig. 6(b). The Bi islands of a low coverage (~0.04) on Pt(poly) certainly promote dehydrogenation path, but still permit the formation of poison. As observed on I/Bi/Pt(poly) in Fig. 6(c), on the other hand, the iodine adsorbed on plain Pt sites of Bi/Pt(poly) prohibits the two FAO paths. Specifically, the serious decrease in FAO current in the presence of adsorbed iodine implies that the FAO efficiency on plain Pt sites is much higher than that on Bi islands. On Bi/Pt(poly), therefore, plain Pt sites around Bi islands (thus modified by Bi) are suggested to promote dehydrogenation path, while those far from Bi islands (hence not modified by Bi) still permit dehydration. Judging from the size of Pt deposits around Bi islands (Fig. 2), the range under the influence exerted by Bi would be ~5 nm, and an electronic effect would account for such a long-range modification. Recalling no irreversible adsorption of Pt ions on plain Pt disk surfaces, the Pt deposits around Bi islands on Pt/Bi/Pt(111) definitely support that Bi islands modify the adjacent plain Pt sites toward Pt ion adsorption as well as FAO.

The FAO efficiency of additional Pt deposits on Bi/Pt(poly) depends on their deposition sites. The FAO behavior of Pt′/I/Bi/Pt(poly) is demonstrated in Fig. 6(d). Specifically, the FAO voltammogram of Pt′/I/Bi/Pt(poly) is similar to that of I/Bi/Pt(poly), but the current in the positive-going scan becomes slightly lager. Thus, the Pt deposits on Bi island are not so effective to slightly increase the FAO current around 0.4 V. As the adsorbed iodine is removed, Pt′/Bi/Pt(poly) restores the paths of dehydrogenation and dehydration with a slightly less FAO efficiency as revealed by the current below 0.4 V and poison oxidation peak at 0.6 V in Fig. 6(e), respectively. This observation definitely confirms that the FAO efficiency of Bi/Pt(poly) is mainly due to the enhancement of dehydrogenation at plain Pt sites modified by Bi and that the Pt deposits on Bi islands marginally contribute to FAO. The low FAO efficiency of the Pt deposits on Bi islands would be due to two reasons: one is that a lateral electronic interaction between Pt and Bi is effective for FAO, while a vertical interaction is not operational, and the other is that a lattice mismatch of Pt deposits Bi islands is not appropriate. Fig. 6(f) shows that Pt/Bi/Pt(poly) is more effective than Bi/Pt(poly) and Pt′/Bi/Pt(poly), indicating that the additional Pt deposits around Bi islands on Pt/Bi/Pt(poly) are quite effective in FAO. Thus, plain Pt sites around Bi islands on a Pt disk enhances FAO most likely via long-range electronic effect. Also, one may argue that Bi next to Pt would be a binding site for formic acid or an intermediate such as formate for the Pt around Bi to enhance FAO. If so, the interaction between Bi and Pt would be a short-range

one, which is not consistent with the observations in this work.

The FAO potential range on I/Bi/Pt(poly) and Pt/I/Bi/Pt(poly) differs from that of dehydrogenation. The FAO current peaks in the presence of iodine on the investigated Bi-modified Pt(poly)s are at ~0.8 V (Fig. 6(c) and (d)), while that of dehydrogenation in the absence of Bi is at the potentials lower than 0.4 V. The particular potential above 0.8 V certainly corresponds to the surface oxidation region as shown in Fig. 5, where dehydration and dehydrogenation do not take place on plain Pt surfaces. Furthermore, the current of ~2 $mA \cdot cm^{-2}$ on I/Bi/Pt(poly) observed in a formic acid solution is much larger than the surface oxidation currents above 0.4 V (< ~0.05 $mA \cdot cm^{-2}$) (Fig. 5), indicating that the current is certainly ascribable to an FAO path occurring on oxidized surfaces of I/Bi/Pt(poly) and Pt/I/Bi/Pt(poly). This particular FAO process occurring at a high potential of ~0.8 V should be distinguished from the well-known FAO routes taking place on metallic surfaces of Pt and Bi-modified Pt below 0.4 V. Therefore, the FAO process of interest has been proposed to be oxidized surface path by us [31,36]. On such oxidized electrode surfaces, some surface oxygen anions formed in the presence of Bi may promote FAO via bifunctional mechanism: for instance, surface oxygen anions (*e.g.*, $O^{\delta-}$, $\delta \leq 2$) may assist to de-hydrogenate HCOOH in some way (or $HCOOH + 2O^{\delta-} \rightarrow CO_2 + 2OH^{(\delta-1)-} + 2e$). It should be noted here that on Pt(poly) disk, the oxidized surface path is always associated with the presence of adsorbed iodine, even though on Bi-modified Pt nanoparticles, it was observed in the absence of adsorbed iodine [31].

For a purpose of comparison, Pt disk electrodes modified with a Bi precursor solution of a 2.6 mM (20 times higher than before) were investigated also. The electrochemically measured coverage of Bi deposits using the Bi precursor solution was ~0.25 (hereafter this particular Bi layer is designated Bi′, *e.g.*, Bi′/Pt disk).

The STM images of Bi′/Pt(111), Pt/Bi′/Pt(111) and Pt′/Bi′/Pt(111) are shown in Fig. S3, Supporting Information. The image of Bi′/Pt(111) (Fig. S3(a)) reveals that the surface is uniformly covered with Bi islands of ~5 nm in diameter. The area fraction of Bi islands on Pt(111) is ~0.67 (although plain Pt sites are not discernible due to a high roughness), while the area fractions of the two- and three atomic-layers high layers are ~0.39 and ~0.19, respectively. These results imply that the Bi precursor solution of the higher concentration results in multiple-layered Bi islands differing from those in Fig. 2(b). On the other hand, the apparent morphologies of Pt/Bi′/Pt(111) and Pt′/Bi′/Pt(111) (Fig. S3(b) and (c)) are not so different from that before Pt deposition. However, the respective area fractions of Pt/Bi′/Pt(111) and Pt′/Bi′/Pt(111) are ~0.74 and ~0.67. In particular, the higher fraction of Pt/Bi′/Pt(111) implies that additional Pt deposits are in the plain Pt sites surrounded by Bi islands. The increments in the area fractions of the two- and three atomic-layers high layers of Pt/Bi′/Pt(111) and Pt′/Bi′/Pt(111) are roughly 0.1 and 0.05, indicating that the amount of Pt deposited on Bi islands is not so high. Thus, it becomes obvious that although the two deposition routes are operational on Bi′/Pt(111), Pt deposition is not so much effective as on Bi/Pt(111).

Fig. 7 presents the FAO behaviors of Bi′/Pt(poly), Pt′/Bi′/Pt(poly) and Pt/Bi′/Pt(poly). The FAO current on Bi′/Pt(poly) at ~0.4 V (Fig. 7(b)) is two times higher than that of Bi/Pt(poly), even though the area fraction of plain Pt sites on Bi′/Pt(poly) (~0.3) is approximately one half of that of Bi/Pt(poly) (~0.7). As plain Pt sites of Bi′/Pt(poly) are blocked by iodine, the FAO current of oxidized surface path appears again at the expense of dehydrogenation current (Fig. 7(c)). Deposition of Pt on I/Bi′/Pt(poly) induces a slight increase in the FAO current, especially around 0.4 V (Fig. 7(d)). After removing the adsorbed iodine from Pt′/I/Bi′/Pt(poly), the FAO current of dehydrogenation on Pt′/Bi′/Pt(poly) resumes, but is less than that on Bi′/Pt(poly) (Fig. 7(e)). Furthermore, the FAO behavior on Pt/Bi′/Pt(poly) (Fig. 7(f)) is similar to that on Pt′/Bi′/Pt(poly). Thus, when the Bi coverage is 0.25, additionally deposited Pt is unfavorable to FAO.

The FAO behavior on Bi-modified Pt(poly), especially associated with additional Pt deposits, depends on the coverage of Bi. Fig. 6 and 7 clearly demonstrate that the FAO current on Bi/Pt(poly) is lower than that of Bi′/Pt(poly). It is also revealed that additional Pt deposits on Bi/Pt(poly) enhance FAO, while those on Bi′/Pt(poly) hamper. When Bi coverage is low, the scattered Bi islands modify the adjacent plain Pt sites to enhance FAO. Furthermore, additional Pt deposits around Bi islands on Pt/Bi/Pt(poly) increase FAO performance, reflecting that the Pt

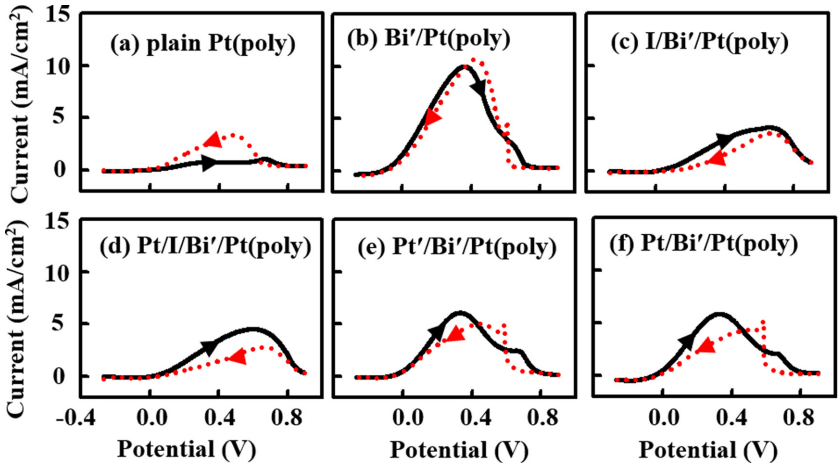

Fig. 7. FAO behaviors of various Bi-modified Pt(poly) electrodes with a Bi coverage of ~0.25 in a solution of 1.0 M formic acid and 0.10 M H_2SO_4: (a) plain Pt(poly), (b) Bi/Pt(poly), (c) I/Bi/Pt(poly), (d) Pt/I/Bi/Pt(poly), (e) Pt′/Bi/Pt(poly), and (f) Pt/Bi/Pt(poly). Scan rate: 50 $mV \cdot s^{-1}$.

deposits are also influenced by Bi. When Bi coverage is high, on the other hand, the Bi islands are so much populated or aggregated to produce small Bi-free plain Pt sites (*i.e.*, Pt ensembles). Consequently, the Pt ensembles of Bi′/Pt(poly) are anticipated to be more seriously modified via electronic effect to increase FAO performance. Indeed, the FAO efficiency of the Pt ensembles is simply calculated to be four times higher than that on Bi/Pt(poly), considering that the area fraction of Pt on Bi′/Pt(111) is approximately one half of that on Bi/Pt(111) and that the observed FAO current on the former is roughly two times higher than that on the latter. If the electronic effect of Bi is the only reason for such a high FAO performance of Bi′/Pt(poly), however, the FAO current on Pt/Bi′/Pt(poly) should increase (analogously to Pt/Bi/Pt(poly)) (Fig. S3), or at least remain constant (if the amount of additionally deposited Pt is not high enough to increase the amount of Pt modified by Bi). In reality, the additional deposition of Pt on Bi′/Pt(poly) regardless of depositing routes results in a decrease in FAO current, implying that the electronic effect is not the only reason. Note that on the less effective Pt′/Bi′/Pt(poly), there is no Pt deposit in its Pt ensembles but there are Pt deposits on Bi islands surrounding the Pt ensembles (see Fig. 7(b) and (e)). Thus, only the specific Pt ensembles on Bi′/Pt(poly) are highly effective in FAO. The additional Pt certainly reduce or remove the advantage of the specific Pt ensembles on Bi′/Pt(poly) for a reason not clearly understood at this moment. Thus, the ensemble effect is suggested to operate only at a Bi coverage high enough to form Pt ensembles. Presuming no ensemble effect on Pt/Bi′/Pt(poly), a comparison of the FAO currents on Bi′/Pt(poly) and Pt/Bi′/Pt(poly) suggests that the contribution of the electronic effect to FAO enhancement on Bi′/Pt(poly) is about one half.

An FAO behavior on Pt nanoparticle (Pt NP) modified with Bi and Pt sequentially deposited in direct route [31] is worthy to address. Deposition of Bi on Pt NP (Bi/Pt NP) using irreversible adsorption to electrochemical coverage of 0.25 enhanced FAO performance by a factor of ~2. When additional deposition of Pt was performed on the Bi/Pt NP (or Pt/Bi/Pt NP), the amount of Pt was significant, and the FAO performance further increased to a value greater by a factor of ~2 referring to that of Bi/Pt NP. In this regard, Pt/Bi′/Pt(poly) and Pt/Bi/Pt NP are quite contrasting in the role of the additional Pt deposits, because Bi deposits on Pt(poly) and Pt NP modify the additional Pt deposits in the opposite directions. Also, it should be emphasized that the FAO behavior via oxidized surface path was observed on Bi/Pt NP and Pt/Bi/Pt NP, while not observed on Bi/Pt(disk) and Pt/Bi/Pt(disk) [40]. However, this work reveals that the presence of iodine on Bi-modified Pt disk is needed to initiate FAO via oxidized surface path. The different FAO behavior on Bi/Pt and Pt/Bi/Pt is most likely due to the physical shapes and sizes of the two Pt substrates [30].

4. Conclusions

In this work, the FAO enhancement on Bi-modified Pt disk was demonstrated to be due to the electronic and ensemble effects by comparing the several Bi-modified Pt disks prepared in a controlled manner. The operational role of Bi depended on its coverage. When the Bi coverage is ~0.04, the Bi islands electronically modified the adjacent plain Pt sites to enhance FAO. When the Bi coverage was ~0.25, the electronic and ensemble effects simultaneously contribute to the observed FAO enhancement. With the aids of the adsorbed iodine, on the other hand, Bi islands and Pt deposits on Bi islands were confirmed not to be effective in FAO below 0.4 V, but to permit FAO via the oxidized surface path. A comparison of the FAO behavior on Pt disk with that on Pt nanoparticle implied that the physical shape and size of Pt modified with Bi might be important in FAO.

Supporting information

Replacement of iodine with CO on plain Pt(poly); replacement of iodine with CO on Bi-modified Pt(poly); EC-STM images of Pt(111) modified with Bi of a high coverage (~0.25).

Supporting information is available at https://doi.org/10.33961/jecst.2022.00514

Acknowledgment

This work was supported by Chungnam National University (2021-0865-01).

References

[1] A. Capon and R. Parsons, *J. Electroanal. Chem.*, **1973**, *45(2)*, 205-231.
[2] C. Rice, R. I. Masel, P. Waszczuk, and T. Barnard, *J. Power Sources*, **2002**, *111(1)*, 83-89.
[3] J. D. Lović, A. V. Tripković, S. L. Gojković, K. D. Popović, D. V. Tripković, P. Olszewski, and A. Kowal, *J. Electroanal. Chem.*, **2005**, *581*, 294-302.
[4] X. Yu and P. G. Pickup, *J. Power Sources*, **2008**, *182(1)*, 124-132.
[5] W. Gao, J. A. Keith, J. Anton, and T. Jacob, *J. Am. Chem. Soc.*, **2010**, *132(51)*, 18377-18385.
[6] A. Boronat-González, E. Herrero, and J. M. Feliu, *Curr. Opin. Electrochem.*, **2017**, *4(1)*, 26-31.
[7] S. Enthaler, J. V. Langermann, and T. Schmidt, *Energy Environ. Sci.*, **2010**, *3*, 1207-1217.
[8] H.-R. M. Jhong, S. Ma, and P. J. A. Kenis, *Curr. Opin. Chem. Eng.*, **2013**, *2(2)*, 191-199.
[9] S. Zhang, P. Kang, and T. J. Meyer, *J. Am. Chem. Soc.*, **2014**, *136(5)*, 1734-1737.
[10] R. Kortlever, I. Peters, S. Koper, and M. T. M. Koper, *ACS Catal.*, **2015**, *5(7)*, 3916-3923.
[11] A. K. Singh, S. Singh, and A. Kumar, *Catal. Sci. Technol.*, **2016**, *6*, 12-40.
[12] M. Neurock, M. Janik, and A. Wieckowski, *Faraday Discuss.*, **2009**, *140*, 363-378.
[13] W. Gao, J. A. Keith, J. Anton, T. Jacob, *Dalton Trans.*, **2010**, *39*, 8450-8456.
[14] M. Osawa, K. Komatsu, G. Samjeske, T. Uchida, T. Ikeshoji, A. Cuesta, C. Gutierrez, *Angew. Chem. Int. Ed.*, **2011**, *50*, 1159-1163.
[15] K. Jiang, H. X. Zhang, S. Z. Zou, and W. B. Cai, *Phys. Chem. Chem. Phys.*, **2014**, *16*, 20360-20376.
[16] Y. Y. Qi, J. Gao, D. J. Zhang, and C. B. Liu, *RSC Adv.*, **2015**, *5*, 21170-21177.
[17] K. Zhang, H. W. Wang, C. Q. Wang, B. B. Yang, F. F. Ren, P. Yang, and Y. K. Du, *Colloids Surf. A*, **2015**, *467*, 211-215.
[18] S. Uhm, H. J. Lee, Y. Kwon, and J. Lee, *Angew. Chem. Int. Ed.*, **2008**, *47(52)*, 10163-10166.
[19] F. Matsumoto, C. Roychowdhury, F. J. Di Salvo, and H. D. Abruna, *J. Electrochem. Soc.*, **2008**, *155*, B148-B154.
[20] N. Kristian, Y. Yan, and X. Wang, *Chem. Commun.*, **2008**, 353-355.
[21] J. Kim and C. K. Rhee, *Electrochem. Commun.*, **2010**, *12(12)*, 1731-1733.
[22] R. Wang, C. Wang, W.-B. Cai, and Y. Ding, *Adv. Mater.*, **2010**, *22(16)*, 1845-1848.
[23] S. Zhang, Y. Shao, G. Yin, and Y. Lin, *Angew. Chem. Int. Ed.*, **2010**, *49(12)*, 2211-2214.
[24] G. Chen, Y. Li, D. Wang, L. Zheng, G. You, C.-J. Zhong, L. Yang, F. Cai, J. Cai, and B. H. Chen, *J. Power Sources*, **2011**, *196(20)*, 8323-8330.
[25] J. V. Perales-Rondón, A. Ferre-Vilaplana, J. M. Feliu, and E. Herrero, *J. Am. Chem. Soc.*, **2014**, *136(38)*, 13110-13113.
[26] A. Ferre-Vilaplana, J. V. Perales-Rondón, J. M. Feliu, and E. Herrero, *ACS Catal.*, **2015**, *5*, 645-654.
[27] T. Duan, R. Zhang, L. Ling, and B. Wang, *J. Phys. Chem. C*, **2016**, *120(4)*, 2234-2246.
[28] D. Li, F. Meng, H. Wang, X. Jiang, and Y. Zhu, *Electrochim. Acta*, **2016**, *190*, 852-861.
[29] J. K. Yoo and C. K. Rhee, *Electrochim. Acta*, **2016**, *216*, 16-23.
[30] J. K. Yoo, M. Choi, S. Yang, B. Shong, H.-S. Chung, Y. Sohn, and C. K. Rhee, *Electrochim. Acta,* **2018**, *273*, 307-317.
[31] H. Lee, Y. S, and C. K. Rhee, *Langmuir*, **2020**, *36(19)*, 5359-5368.
[32] M. Choi, C.-Y. Ahn, H. Lee, J. K. Kim, S.-H. Oh, W. Hwang, S. Yang, J. Kim, O.-H. Kim, I. Choi, Y.-E. Sung, Y.-H. Cho, C. K. Rhee, and W. Shin, *Appl. Catal.*

B., **2019**, *253*, 187-195.
[33] J. Kim and C. K. Rhee, *J. Solid State Electrochem.*, **2013**, *17(12)*, 3109-3114.
[34] D. Zhao, Y.-H. Wang, and B.-Q. Xu, *J. Phys. Chem. C*, **2009**, *113(49)*, 20903-20911.
[35] G.-R. Zhang, D. Zhao, Y.-Y. Feng, B. Zhang, D. S. Su, G. Liu, and B.-Q. Xu, *ACS Nano*, **2012**, *6(3)*, 2226-2236.
[36] H. Lee, Y. J. Kim, Y. S, and C. K. Rhee, *J. Electrochem. Sci. Technol*., **2021**, *12(3)*, 323-329.
[37] D. Zurawski, L. Rice, M. Hourani, and A. Wieckowski, *J. Electroanal. Chem.*, **1987**, *230(1-2)*, 221-231.
[38] J. Lee, J. K. Yoo, J. Kim, Y. Sohn, and C. K. Rhee, *Electrochim. Acta*, **2018**, *290*, 244-254.
[39] M. D. Macia, E. Herrero, J. M. Feliu, and A. Aldaz, *J. Electroanal. Chem.*, **2001**, *500(1-2)*, 498-509.
[40] A. López-Cudero, F. J. Vidal-Iglesias, J, Solla-Gullón, E, Herrero, A. Aldaz, and J. M. Feliu, *Phys. Chem. Chem. Phys.*, **2009**, *11*, 416-424.